Submitted to the
XXXIII International Conference On High Energy Physics
26 July - 2 August, 2006, Moscow, Russia

Abstract: **Session: QCD soft interactions/QCD hard interactions**

Diffractive photoproduction of J/ψ mesons with large momentum transfer at HERA

ZEUS Collaboration

Abstract

The proton-dissociative diffractive photoproduction of J/ψ mesons has been studied in ep collisions with the ZEUS detector at HERA using an integrated luminosity of 112 pb^{-1}. The cross section has been measured as a function of the centre-of-mass energy of the photon-proton system and of the squared four-momentum transfer at the proton vertex. The results are compared to perturbative QCD calculations based on BFKL and DGLAP evolution equations.

1 Introduction

General properties of proton-dissociative photoproduction of vector mesons at large squared four-momentum transfer t have been successfully described by the pQCD-based models where a nearly-real photon fluctuates into a vector meson which then interacts with a single parton in the proton via color singlet exchange. Such an exchange can be either two gluons [1] (Fig. 1, left) or a gluon ladder (Fig. 1, right). The latter can be described by standard DGLAP [2] or BFKL [3–5] low-x QCD evolution equations.

In pQCD models t, or the meson mass in the case of the J/ψ, provides a hard scale required for the perturbative treatment of QCD processes. In particular, these models predict t distributions that are relatively hard compared to elastic vector meson photoproduction. With a reasonable choice of two parameters, the model using BFKL exchange could describe the shapes and magnitude of the differential cross section as a function of t for ρ, ϕ and J/ψ mesons [6].

The pQCD models using different exchanges and evolution equations differ, however, in the predicted energy dependence of $d\sigma/dt$: two-gluon exchange yields energy independent cross sections [1], gluon ladder with DGLAP evolution predits practically no energy dependence [2] whereas BFKL evolution leads to cross sections that rise significantly with increasing energy [4, 5]. The latter rise has been observed in J/ψ photoproduction at $|t| > 5\,\mathrm{GeV}^2$ [7] suggesting onset of BFKL dynamics at larger $|t|$. It is investigated also in this paper in which the differential cross section $d\sigma/dt$ and its energy dependence are presented for the diffractive photoproduction process, $\gamma p \rightarrow J/\psi\, Y$, where Y is the proton dissociative system. The data were taken in a photon-proton centre-of-mass (CMS) energy range $50 < W < 150\,\mathrm{GeV}$ and extend up to $|t| = 20\,\mathrm{GeV}^2$. These results are compared to predictions of the BFKL model [5] and DGLAP calculations in leading logarithmic approximation [2].

2 Experimental conditions

The data used in this analysis were collected in 1996 - 2000 from ep interactions with the ZEUS detector [8] at HERA, which operated with a proton beam energy of 820(920) GeV and a positron beam energy of 27.5 GeV, and correspond to an integrated luminosity of $112\,\mathrm{pb}^{-1}$. The main components used for this analysis are the central tracking detector (CTD) [9], the uranium-scintillator calorimeter (CAL) [10], the muon chambers [11], the proton remnant tagger (PRT) [12] and the forward plug calorimeter (FPC) [13].

3 Kinematics and cross sections

The process in question is the proton-dissociative J/ψ production in ep interactions:

$$e(k)p(P) \to e(k')J/\psi(v)Y(P'),$$

where k, k', P, P' and v are the four-momenta of the incident positron, scattered positron, incident proton, diffractive nucleonic system Y and J/ψ, respectively (Fig. 2). The kinematic variables used to describe this process are:

- $Q^2 = -q^2 = -(k-k')^2$, the negative squared four-momentum of the exchanged photon;
- $W^2 = (q+P)^2$, the squared CMS energy of the photon-proton system;
- $-t = (P'-P)^2 = (v-q)^2$, the squared four-momentum transfer at the proton vertex;
- $z = (P \cdot v)/(P \cdot q)$, event elasticity, the fraction of virtual photon energy transferred to the J/ψ in the proton rest frame.

The kinematic variables were reconstructed using momenta of J/ψ decay products.

For the photon virtualities, $Q^2 \approx 0.01\,\mathrm{GeV}^2$, covered by this measurement, the differential ep cross section can be expressed as

$$\frac{d^2\sigma^{ep\to eJ/\psi Y}}{dydQ^2} = \Gamma_T(y, Q^2)\sigma^{\gamma p}(y)$$

where Γ_T is the flux of the transverse virtual photons. The photon-proton cross section can be extracted from the ep cross section since one is related to the other by means of the flux factor generated at the leptonic vertex which can be integrated over the y and Q^2 covered by the measurement.

4 Reconstruction and selection of events

The signature of proton dissociative J/ψ photoproduction, $ep \to eJ/\psi Y$ consists of two oppositely charged muons from J/ψ decay, the dissociated proton and the lack of the scattered electron in the main detector. The electron is scattered at small angle and escapes undetected down the beampipe. The low mass hadronic states originating from scattered proton are registered in the forward part of the calorimeter or in the forward detectors.

The events were selected online by the ZEUS trigger system. The di-muon sample was triggered by requiring at least one track in the CTD matched to an energy deposit in the

CAL. The energy deposit was required to be consistent with a minimum ionizing particle and associated to a signal in the muon chambers.

Further selection made offline required two energy deposits in the CAL associated with the two candidate leptons from the J/ψ decay. To select events with dissociation of the proton, an energy deposit above 400 MeV with $|\eta| > 2.1$ [1] in the forward part of the CAL was required and a signal in the PRT (for 1996-1997 data sample) or an energy deposit with $E_{FPC} > 1\,\mathrm{GeV}$ in the FPC (for 1998-2000 data sample). Events with additional energy deposits with $|\eta| < 2.1$ above the noise level (300 MeV) and not associated with lepton candidates were rejected.

In order to compare cross sections with theoretical predictions and former measurements, the additional cut $z > 0.95$ was applied. This cut ensures diffractive character of the interaction and also restricts the invariant mass of the system Y to be $M_Y < 30\,\mathrm{GeV}$ through relation $z = 1 - (M_Y^2 - t)/W^2$. The measurement of z is obtained from $(E - p_z)_{J/\psi}/\Sigma(E-p_z)$ where $\Sigma(E-p_z)$ is calculated from all energy deposits in the CAL above the noise level including the decay products of the J/ψ.

Since the typical Q^2 is small, it can be neglected in the reconstruction of the other kinematic variables. In particular, the squared four-momentum transfer $|t|$ was assumed to be equal to the squared transverse-momentum of the di-lepton system resulting from the J/ψ decay. Events were required to be in a kinematic range where the properties of the final state particles are properly measured and the acceptance is well defined, which is satisfied for $2.6 < M_{\mu\mu} < 3.5\,\mathrm{GeV}$, $1 < |t| < 20\,\mathrm{GeV}^2$, $50 < W < 150\,\mathrm{GeV}$.

5 Monte Carlo simulation

The acceptance and the effects of the detector response were determined using samples of Monte Carlo (MC) events. All generated events were passed through the standard ZEUS detector simulation, based on GEANT 3.13 [14] program, the ZEUS trigger simulation package, and through the same reconstruction and analysis programs as the data.

The process $ep \to eJ/\psi Y$ was modelled using the generator EPSOFT [15, 16]. The $\gamma p \to J/\psi Y$ cross section was parametrised as $f(t)(M_Y^2)^{-\beta(t)}$. The MC samples were tuned to describe the FCAL and FPC energy distributions, which are sensitive to M_Y^2, yielding $\beta(t) = \exp(0.25 - 0.37|t|)$. The MC t distribution was also reweighted to obtain the power-like dependence of $d\sigma/dt$ as measured in the data.

A non-resonant background due to the $\gamma\gamma$ fusion process, $ep \to e\mu^+\mu^- Y$, where one

[1] Pseudorapidity $\eta = -\ln\tan\frac{\theta}{2}$, where θ is the polar angle measured with respect to the collision axis.

of photons is emitted by electron and the second photon is radiated off the proton was simulated using the generator GRAPE-DILEPTON 1.1 [17].

6 Results

The invariant mass distribution of the $\mu^+\mu^-$ pairs is presented in Fig.3. The MC distribution of the J/ψ signal is also shown as well as the QED background. After all selection cuts almost 3000 di-muon events were left in the mass range $2.6 < M_{\mu^+\mu^-} < 3.5$ GeV. A non-resonant background from $\gamma\gamma \to l^+l^-$ events was estimatated in each bin using the GRAPE, normalised to the luminosity of the data.

The differential cross section $d\sigma(\gamma p \to J/\psi\ Y)/d|t|$ was measured as a function of $|t|$ in the range $1 < |t| < 20\,\mathrm{GeV}^2$, $50 < W < 150\,\mathrm{GeV}$ and $z > 0.95$. The data were compared to the H1 measurement [7], as shown in Fig. 4. The ZEUS cross section is higher than the H1 results and this difference decreases with the rise of $|t|$. In Fig. 5 the $|t|$ dependence is compared with theoretical predictions of pQCD models. The pQCD model with BFKL evolution [5] provides calculations with leading logarithmic (LL) approximation as well as with non-leading corrections (nonL) with fixed and running α_s. The model with DGLAP evolution gives predictions in the LL approximation [2] in the range of model validity $|t| < M^2_{J/\psi}$. Parameters of both pQCD models were chosen to describe the previous HERA measurements, as described in [7]. The pQCD predictions with BFKL LL and BFKL nonL with fixed α_s as well as DGLAP LL calculations generally describe the $|t|$ dependence of the cross section but rather underestimate its magnitude, while the BFKL nonL calculations with running α_s give $|t|$ dependence steeper and are unable to describe the data across the whole range of $|t|$.

The cross section $\sigma^{\gamma p \to J/\psi Y}$ was measured as a function of W in four bins of $|t|$ as it is shown in Fig. 6. The cross sections were fitted to a dependence $\sigma \propto W^{\delta}$. The measured values of δ rise with rising $|t|$ and show similar behaviour as the H1 reported [7]. In the Regge formalism, the differential cross section can be expressed as $d\sigma/dt \propto W^{4(\alpha_{IP}(t)-1)}$, where $\alpha_{IP}(t)$ is Pomeron trajectory. The value of $\alpha_{IP}(t)$ for each value of t is obtained from $\alpha_{IP} = (\delta + 4)/4$. The Pomeron trajectory is usually parametrised as a linear form $\alpha_{IP}(t) = \alpha_{IP}(0) + \alpha'_{IP} \cdot t$. Fit performed in four bins of t yields an intercept $\alpha_{IP}(0) = 1.153 \pm 0.048_{stat} \pm 0.039_{syst}$ and a slope $\alpha'_{IP} = -0.020 \pm 0.014_{stat} \pm 0.010_{syst}$. These values are very similar to the values obtained in the H1 data. They are quite different from parametrisation of the 'soft' Pomeron [18] but are consistent with prediction of BFKL Pomeron [19, 20]. In Fig. 7 the comparison with the H1 is presented. The ZEUS data are higher than the H1 cross sections, the effect being weaker at higher $|t|$. The data are also compared to the theoretical predictions, see Fig. 8, which are at the moment available for $|t| > 2\,\mathrm{GeV}^2$ and in the case of BFKL based model, for fixed α_s. The DGLAP LL predictions are not able to describe the W dependence while the BFKL LL reproduces quantitatively rise of the cross section.

To summarise, the differential cross section $d\sigma/dt$ for proton-dissociative J/ψ photoproduction in the kinematic region $50 < W < 150$ GeV and $1 < |t| < 20$ GeV^2 is reproduced semi-quantitatively by pQCD BFKL LL and nonL calculations with fixed strong coupling, while the predictions with running α_s are too steep. The data for $|t| < M^2_{J/\psi}$ are well described by a model based on DGLAP evolution. The cross section rises significantly with increasing energy W, the higher $|t|$ the stronger the rise. This behaviour is reproduced by the quoted BFKL model but not by DGLAP calculations. Effective Pomeron trajectory was estimated yielding intercept $\simeq 1.15$ and slope consistent with zero.

References

[1] D. Yu. Ivanov et al., Phys. Lett. **B478**, 101 (2000).

[2] E. Gotsman et al., Phys. Lett. **B532**, 37 (2002).

[3] J. Bartels et al., Phys. Lett. **B375**, 301 (1996).

[4] J. R. Forshaw and G. Poludniowski, Eur. Phys. J. **C26**, 411 (2003).

[5] R. Enberg et al., Eur. Phys. J. **C26**, 219 (2003).

[6] ZEUS Coll., S. Chekanov et al., Eur. Phys. J. **C26**, 389 (2003).

[7] H1 Coll., A. Aktas et al., Phys. Lett **B568**, 205 (2003).

[8] ZEUS Coll., U. Holm (ed.), *The ZEUS Detector*. Status Report (unpublished), DESY (1993), available on `http://www-zeus.desy.de/bluebook/bluebook.html`.

[9] N. Harnew et al., Nucl. Inst. Meth. **A 279**, 290 (1989);
B. Foster et al., Nucl. Phys. Proc. Suppl. **B 32**, 181 (1993);
B. Foster et al., Nucl. Inst. Meth. **A 338**, 254 (1994).

[10] M. Derrick et al., Nucl. Inst. Meth. **A 309**, 77 (1991);
A. Andresen et al., Nucl. Inst. Meth. **A 309**, 101 (1991);
A. Caldwell et al., Nucl. Inst. Meth. **A 321**, 356 (1992);
A. Bernstein et al., Nucl. Inst. Meth. **A 336**, 23 (1993).

[11] G. Abbiendi et al., Nucl. Inst. Meth. **A 333**, 342 (1993).

[12] ZEUS Coll., J. Breitweg et al., Z. Phys. **C 75**, 421 (1997).

[13] ZEUS coll., FPC group, A. Bamberger et al., Nucl. Inst. Meth. **A 450**, 235 (2000).

[14] R. Brun et al., *GEANT 3.13*, 1987. CERN DD/EE/84-1.

[15] M. Kasprzak. Ph.D. Thesis, Warsaw Univ., Warsaw, Poland, Report DESY F35D-96-16, 1996.

[16] L. Adamczyk. Ph.D. Thesis, Univ. of Mining and Metallurgy, Cracow, Poland, Report DESY-THESIS-1999-045, 1999.

[17] T. Abe, Comp. Phys. Comm. **136**, 126 (2001).

[18] A. Donnachie and P.V. Landshoff, Phys. Lett. **B 348**, 213 (1995).

[19] S.J. Brodsky et al., JETP Lett. **70**, 155 (1999).

[20] N.N. Nikolaev, B.G. Zakharov and V.R. Zoller, Phys. Lett. **B 366**, 337 (1996).

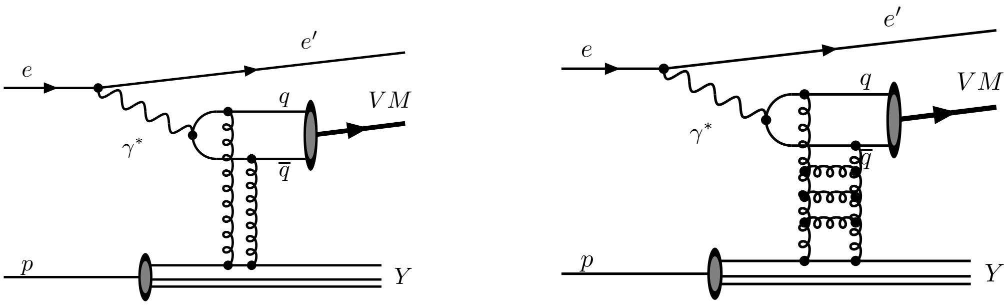

Figure 1: *Left: the pQCD diagram for proton-dissociative vector-meson electro-production via two-gluon exchange. Right: the pQCD diagram with gluon ladder exchange.*

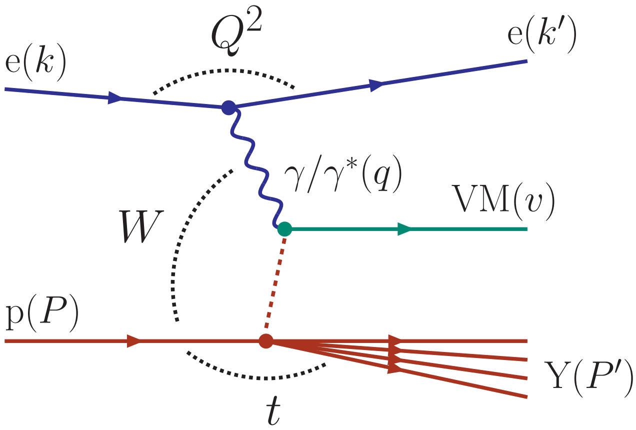

Figure 2: *Schematic diagram of proton-dissociative J/ψ production in ep interactions, $ep \rightarrow eJ/\psi\ Y$.*

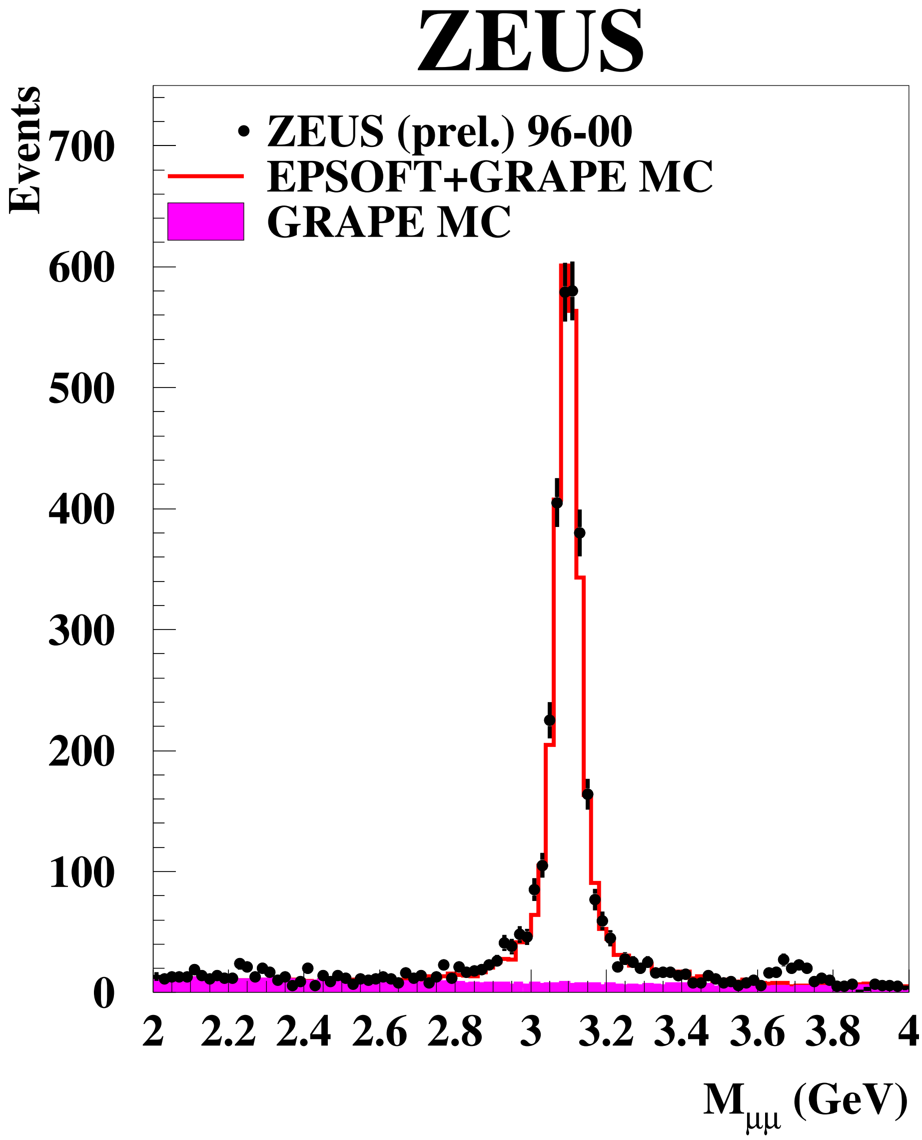

Figure 3: *The invariant mass spectrum for* $J/\psi \rightarrow \mu^+\mu^-$ *in the kinematic range* $1 < |t| < 20\,GeV^2$, $50 < W < 150\,GeV$ *and* $z > 0.95$. *The data are compared to the MC distributions. The shaded histogram represents the* $ep \rightarrow e\mu^+\mu^-Y$ *background as simulated by* GRAPE. *The open histogram represents the sum of* J/ψ *and background MC events.*

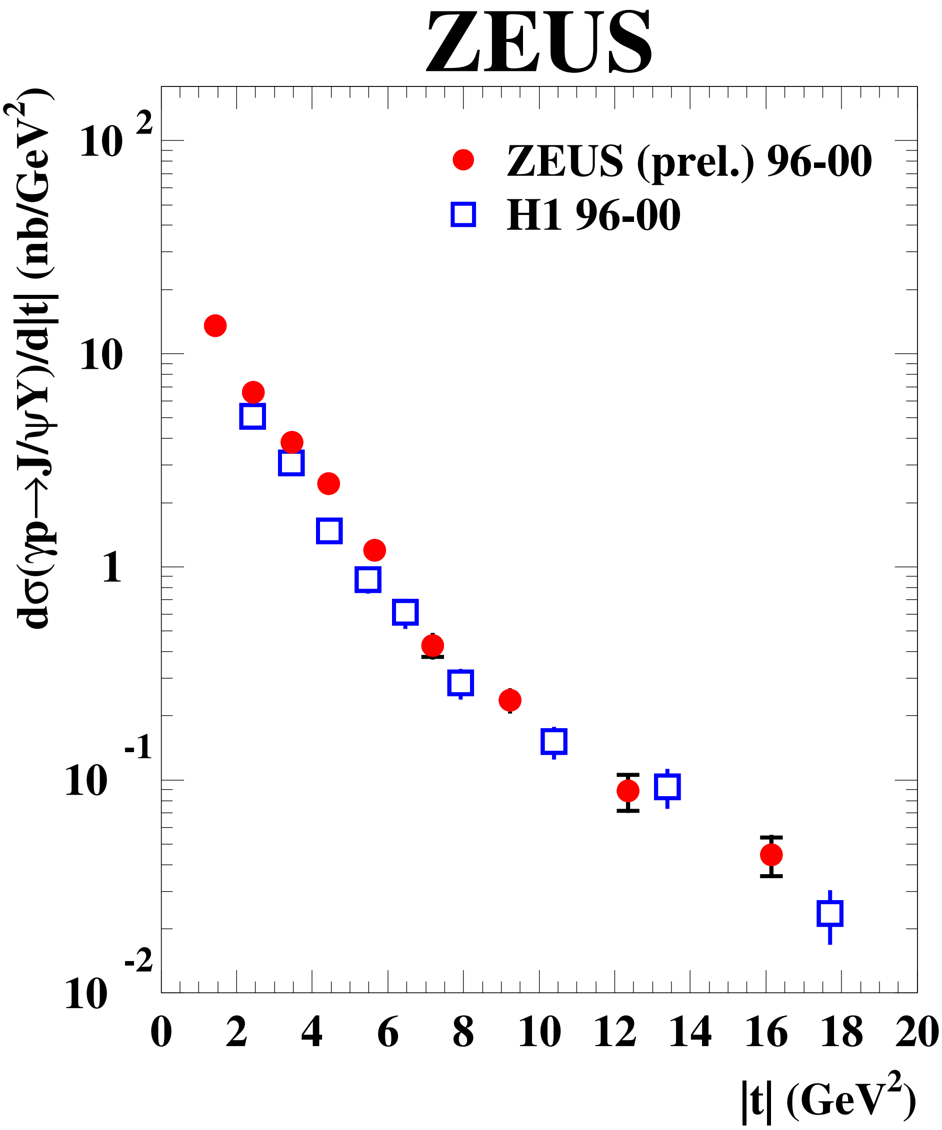

Figure 4: *The differential cross section $d\sigma/d|t|$ for the process $\gamma p \to J/\psi\ Y$ calculated for $1 < |t| < 20\ GeV^2$, $50 < W < 150\ GeV$ and $z > 0.95$. The comparison with the H1 results (open dots) is shown. The inner bars represent the statistical uncertainty and the outer represent the statistical and systematic uncertainty added in quadrature.*

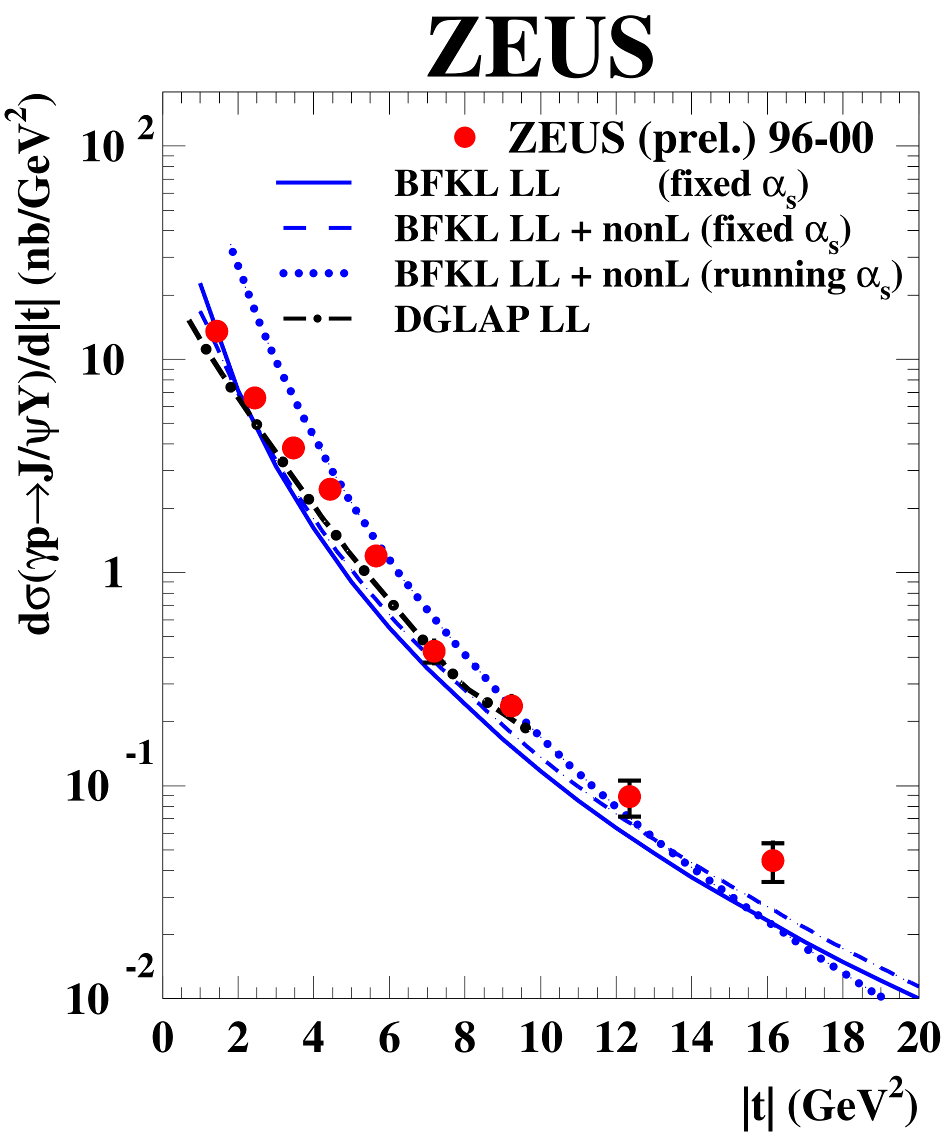

Figure 5: *The differential cross section $d\sigma/d|t|$ for the process $\gamma p \rightarrow J/\psi\ Y$ calculated for $1 < |t| < 20\,GeV^2$, $50 < W < 150\,GeV$ and $z > 0.95$. The inner bars correspond to the statistical uncertainty and the outer to the statistical and systematic uncertainty added in quadrature. The solid line represents the results of BFKL LL with fixed α_s and the dashed(dotted) line – including non-leading corrections (nonL) with fixed(running) α_s. The dashed-dotted curve is a prediction based on DGLAP LL calculations.*

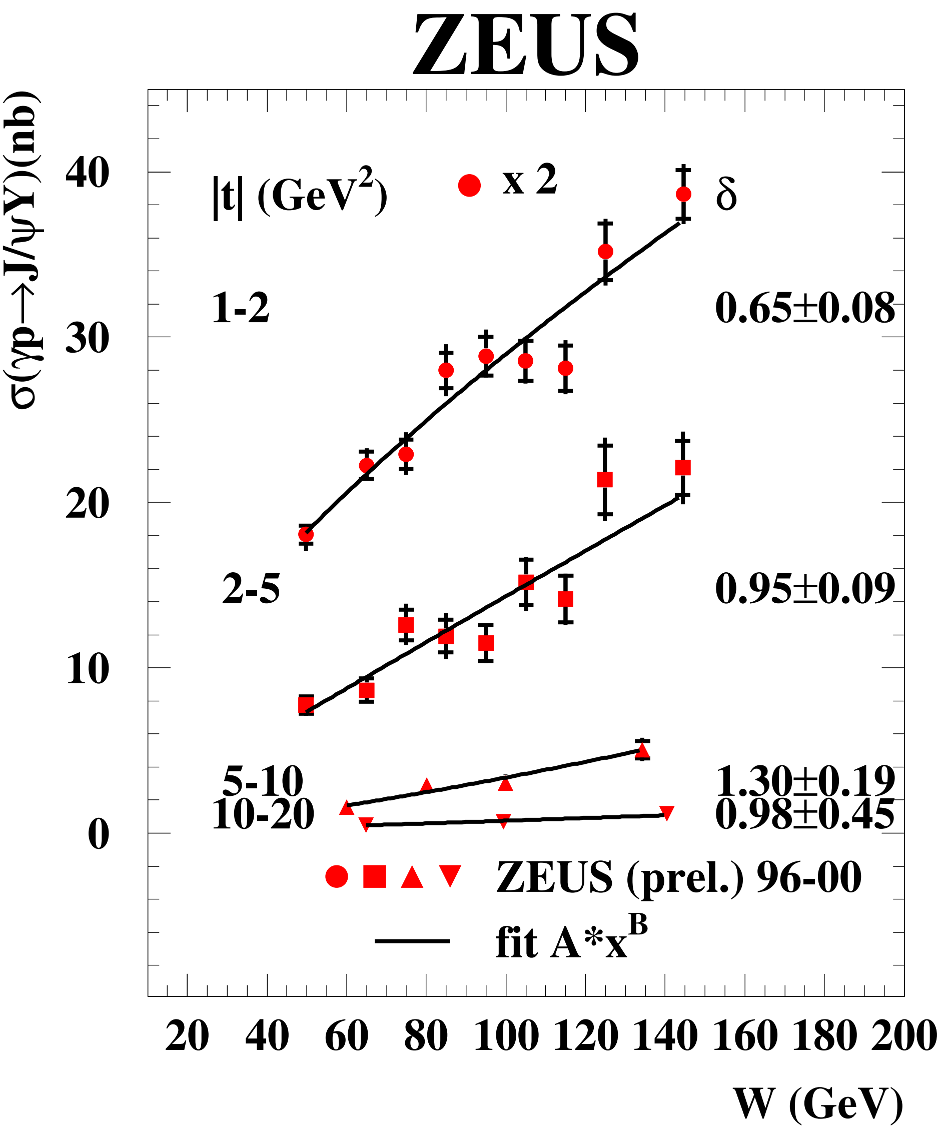

Figure 6: *The cross section as a function of W in four intervals of $|t|$ for $z > 0.95$. The inner bars correspond to the statistical uncertainty and the outer to the statistical and systematic uncertainty added in quadrature. The solid lines are the results of the fit to the form $\sigma \propto W^{\delta}$. The values of power δ are also indicated.*

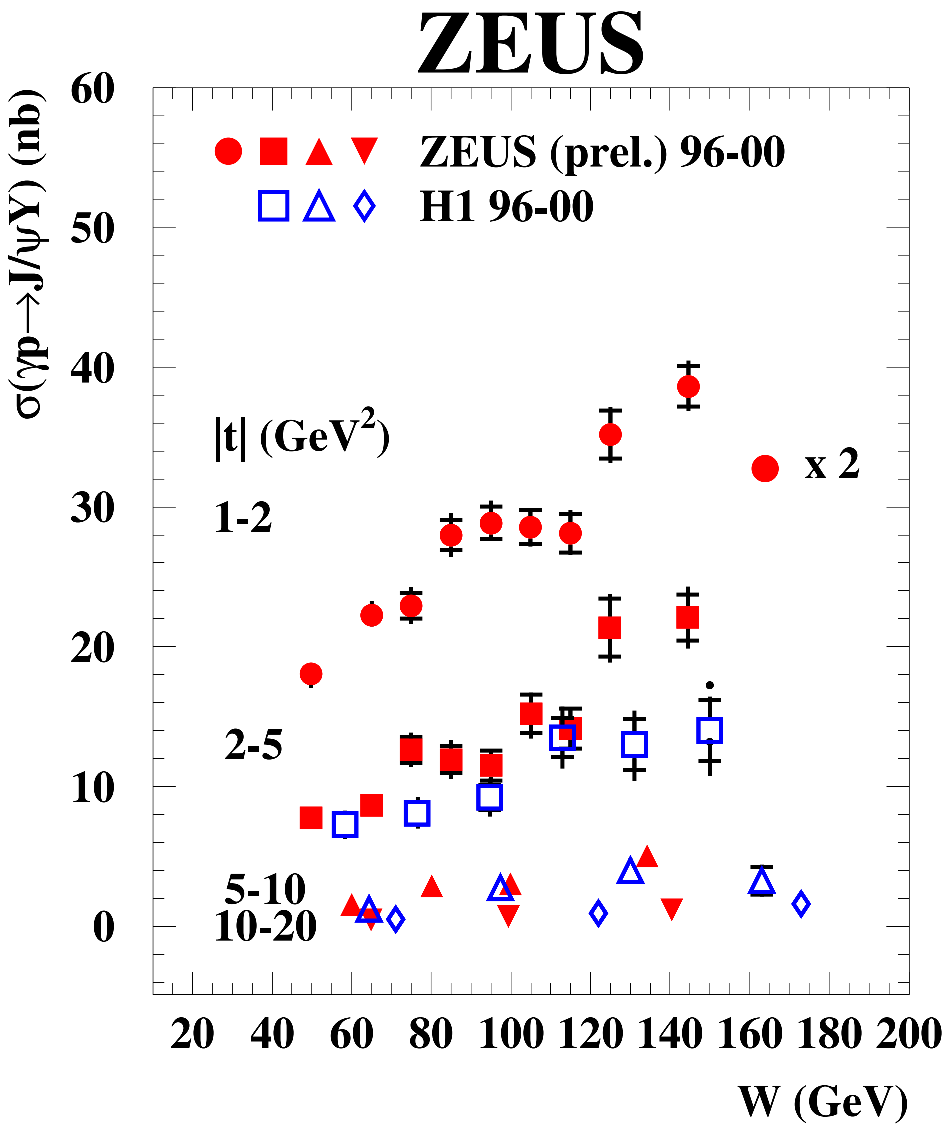

Figure 7: *The cross section as a function of W in four intervals of $|t|$ for $z > 0.95$. The inner bars correspond to the statistical uncertainty and the outer to the statistical and systematic uncertainty added in quadrature. The comparison with the H1 results is shown.*

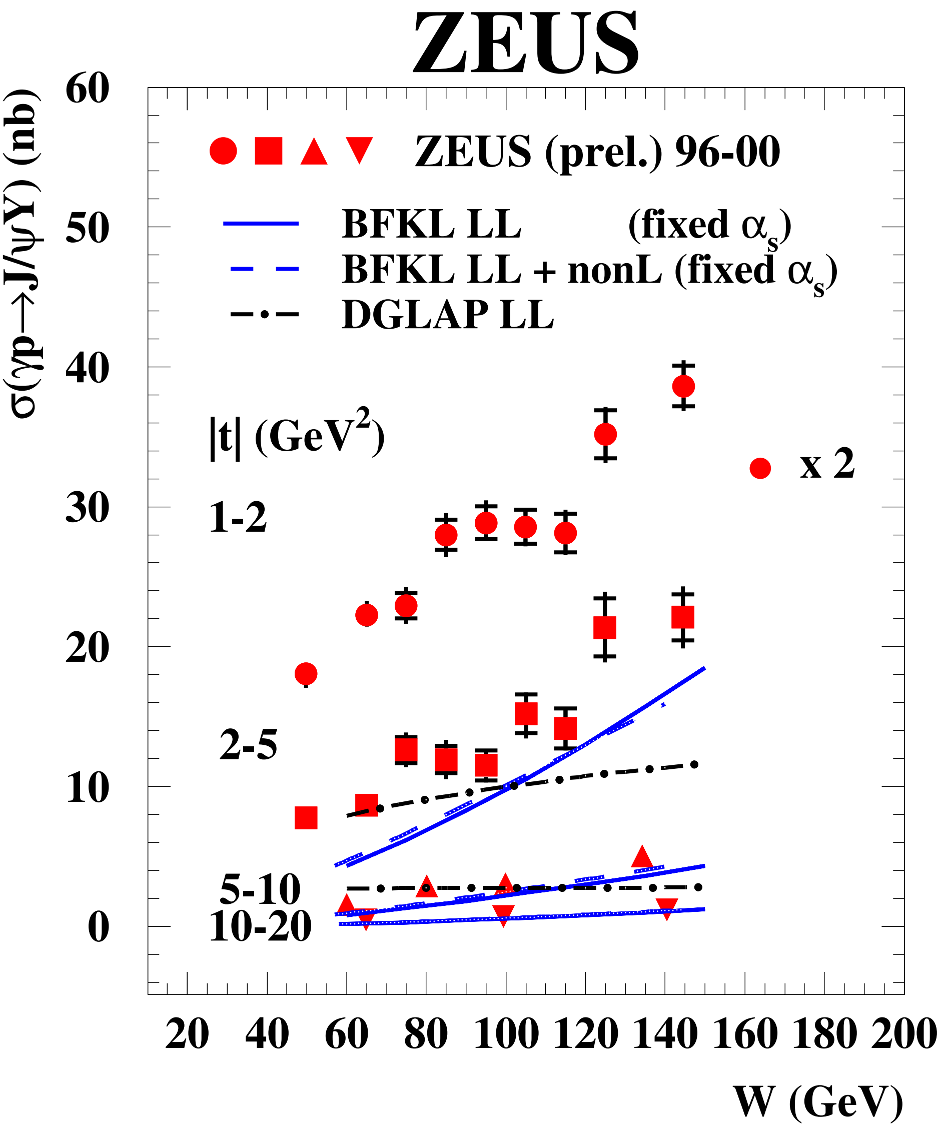

Figure 8: *The cross section as a function of W in four intervals of $|t|$ for $z > 0.95$. The inner bars correspond to the statistical uncertainty and the outer to the statistical and systematic uncertainty added in quadrature. The solid line shows the prediction of BFKL LL calculations and the dashed line corresponds to the predictions including also the nonleading corrections for fixed α_s. The dashed-dotted curve represents the DGLAP LL based calculations.*